11. P. J. Roache, Computational Fluid Dynamics, Hermosa (1976).
12. L. J. Segerlind, Applied Finite Elements Analysis, Wiley (1976).

PLANE TURBULENT WAKE WITH ZERO EXCESS MOMENTUM

Yu. M. Dmitrenko, I. I. Kovalev,
N. N. Luchko, and P. Ya. Cherepanov

UDC 532.517.4

A plane momentumless wake is investigated on the basis of numerical computations by the $\overline{u_i u_j}$–ε model of turbulence and an aerodynamic experiment.

1. Introduction. The turbuient wake behind a flat body constantly attracts the attention of researchers not only because of the numerous technical applications but also as one of the simplest modifications of free shear flow convenient for the confirmation of moder semi-empirical turbulence models. In a number of engineering installations, for instance, in atomizers, mixing units, flame stabilizers, jet flaps, etc., the wakes are formed under conditions of jet efflux from holes located in the root area of streamlined bodies. Here, dependent on the velocity of jet efflux, coflows with a different magnitude of the excess mementum are realized

$$I = \rho \int_0^\infty [U_1 (U_1 - U_\infty) + \overline{u_1^2} - \overline{u_2^2}]\, dx_2. \tag{1}$$

Of special interest is the particular case of such a coflow when the excess momentum equals zero, which corresponds to the condition of equality of the hydrodynamic drag of the streamlined body and the reactive thrust produced by the jet.

In contrast to axisymmetric flow, the number of papers devoted to investigation of a plane wake with zero excess momentum is quite limited. The results of a self-similar analysis for $I = 0$ is contained in [1-4]. The self-similar analysis permits expression of the exponent in the dampling laws of the wake characteristics in terms of one unknown parameter whose magnitude is either determined from experiment [2, 3] or calculated analytically by using certain additional assumptions (for instance, about the constancy of the turbulent viscosity across the wake [1, 4]). A plane coflow with zero excess momentum was investigated experimentally in just one paper [5]. Average velocity profiles were measured in comparative detail therein while the fluctuating characteristics are represented by turbulent energy and tangential stress profiles in just one section. In this connection, available experimental data are inadequate for a critical estimate of the results of self-similar analysis.

Qualitatively, the results of [1-5] are in agreement and show that in principle, the differences in the evolution of the wake characteristics for $I = 0$ and $I \neq 0$ are inherent not only to axisymmetric but also plane wakes. In particular, the defect in the mean velocity damps out in proportion to the kinetic energy of the fluctuations. At a certain distance from the streamlined body the turbulent energy generation becomes negligibly small as compared with its dissipation rate and the turbulent Reynolds number decreases downstream (in contrast to the case $I \neq 0$).

As regards the quantitative estimates, the results of the above-mentioned papers differs substantially. For example, the following estimates $n_u = -0.75$ [1, 5], $n_u = -1.11$ [4], $n_u = -1.5$ [2, 3] are obtained for the exponent n_u in the self-similar law of velocity defect damping. Just as radically different are the exponents for the other characteristics also. Taking account of the known constraints of the self-similarity analysis methods and the contradictions in the quantitative results obtained by using them, as well as the absence of detailed experimental data, results of an aerodynamic experiment and a numerical computation utilizing a multiparametric differential model of turbulence are used to determine the regularities of the evolution of the characteristics of a plane turbulent wake with zero

A. V. Lykov Institute of Heat and Mass Transfer, Academy of Sciences of the Belorussian SSR, Minsk. Translated from Inzhenerno-Fizicheskii Zhurnal, Vol. 52, No. 5, pp. 743-751, May, 1987. Original article submitted March 26, 1986.

 0022-0841/87/5205-0536$12.50

excess momentum in this paper. On the one hand, this permits estimation of the confidence in the mathematical model and the method of numerical integration. On the other, the theoretical and experimental results supplement each other; characteristics are determined in the tests which are not described by the system of model equations (for instance, all three intensity components of the turbulent velocity fluctuations) at the same time those quantities are computed which are difficult to measure with sufficient accuracy (for example, the velocity defect and friction stress at large distances downstream).

2. Experimental Installation and Apparatus

The experiments were conducted in wind tunnel with covered working section 80 × 80 × 1200 mm in size [6]. The model in the form of a rectangular hollow wing was installed at zero angle of attack at the beginning of the tunnel working section. The wing with 74-mm span had a symmetric profile with chord $l = 100$ and relative thickness $d/l = 0.1$. A 2-mm-wide slot was along the model trailing edge and an air jet was injected through it into the wake. The air to produce it was supplied to the wing cavity from a special high-pressure test stand. The measurements were performed for a free-stream velocity $U_\infty = 14.1$ m/sec ($R_\infty = U_\infty d/\nu = 0.93 \cdot 10^4$). The tunnel construction assured constancy of the pressure along the working section with ±0.2% accuracy (with the exception of the domain where the model was installed). The degree of free-stream turbulence was approximately 0.3%. The momentumless flow regime was assured by selecting the jet velocity and was checked by the magnitude of the integral computed at several wake sections where the contribution of the normal Reynolds stresses could be neglected ($x_1/d \geq 6$).

The mean velocity was determined by a combined Pito–Prandtl tube with receiving hole diameter for the total head of 0.8 mm and outer diameter 1.7 mm on which the pressure drop was checked by a MKV-250 micromanometer to 0.1-Pa accuracy. The turbulence characteristics were measured by thermoanemometric apparatus of the firm "DISA" (type "55D"). It had thermoanemometers, linearizers, filters, an effective-value voltmeter and a correlator. Serial probes with one or two crossed hairs 55P01 and 55P61, for which the sensors had a 5-μm diameter and 1.2-mm length were used. To measure the microscale an analog differentiator with working frequency band from 0 to 40 kHz was used. The values obtained for the microscale and the dissipation functions were corrected by taking account of the limited resolution of probe hairs as well as the background fluctuations and noise of the apparatus by a method described in [7].

3. System of Model Equations

The turbulent velocity field of a plane momentumless wake was computed on the basis of a semiempirical model, taking account of the flow singularities due to the rapid decrease in the turbulent Reynolds number R_λ downstream. A closed system of equations is proposed in the monograph [4] and is used in [8] for numerical modeling of the characteristics of an axisymmetric wake with zero excess momentum. Using the free-stream velocity U_∞ and the transverse body dimension d as characteristic parameters, we introduce the dimensionless variables

$$x = \frac{x_1}{d};\ y = \frac{x_2}{d};\ U = \frac{\Delta U}{U_\infty} = \frac{U_1 - U_\infty}{U_\infty};\ V = \frac{U_2}{U_\infty};$$

$$E = \frac{\overline{u_i u_i}}{U_\infty^2} = \frac{q^2}{U_\infty^2};\ R_{ij} = \frac{\overline{u_i u_j}}{U_\infty^2};\ D = \frac{\varepsilon d}{U_\infty^3};\ \varepsilon = \nu \left(\frac{\overline{\partial u_i}}{\partial x_k}\right)^2$$

The system of model equations takes the following form in the boundary-layer approximation

$$\frac{\partial U}{\partial x} + \frac{\partial V}{\partial y} = 0,\ (1+U)\frac{\partial U}{\partial x} + V\frac{\partial U}{\partial y} =$$

$$= \frac{\partial}{\partial y}\left(\frac{1}{R_\infty}\frac{\partial U}{\partial y} - R_{12}\right) - \frac{\partial}{\partial x}(R_{11} - R_{22}) = 0,$$

$$(1+U)\frac{\partial E}{\partial x} + V\frac{\partial E}{\partial y} = \frac{\partial}{\partial y}\left[\left(\frac{1}{R_\infty} + 0{,}03\frac{E^2}{D}\right)\frac{\partial E}{\partial y}\right] - 2R_{12}\frac{\partial U}{\partial y} - 2D = 0,$$

$$(1+U)\frac{\partial R_{12}}{\partial x}+V\frac{\partial R_{12}}{\partial y}=\frac{\partial}{\partial y}\left[\left(\frac{1}{R_\infty}+0{,}03\frac{E^2}{D}\right)\frac{\partial R_{12}}{\partial y}\right]-$$

$$-\gamma E\frac{\partial U}{\partial y}-2S_uR_{12}\frac{D}{E}=0,\ (1+U)\frac{\partial D}{\partial x}+V\frac{\partial D}{dy}=$$

$$=\frac{\partial}{\partial y}\left[\left(\frac{1}{R_\infty}+0{,}02\frac{E^2}{D}\right)\frac{\partial D}{\partial y}\right]-F_u\frac{D^2}{E}-b_u\frac{D}{E}R_{12}\frac{\partial U}{\partial y}=0, \qquad (2)$$

$$S_u=f_u+2{,}8(1-f_u),\ \gamma=0{,}14+0{,}2f_u,\ F_u=\frac{11}{3}-\frac{13}{15}f_u,\ b_u=1{,}45,$$

$$f_u=1-\frac{2}{1+\sqrt{1+\frac{1800}{R_\lambda^2}}},\ R_\lambda=\frac{q\lambda}{\nu},\ \lambda^2=\frac{5\nu q^2}{\varepsilon}.$$

Given as initial conditions in the formulation of the boundary-value problem were the experimental profiles of the functions being modeled in the section $x_1/d = 6$, where the boundary-layer approximation is known to be satisfied. The remaining functions have zero derivatives on the plane of symmetry $V(0, x) = R_{12}(0, x) = 0$. On the outer boundary-layer boundary ($y = \delta$) the velocity defect $U(\delta, x)$ and the tangential stress $R_{12}(\delta, x)$ vanish, while $E(\delta, x)$ and $D(\delta, x)$ are determined by the state of the external turbulent flow. It is assumed that the free stream is isotropic and degenerating, where $E_\infty = E(\delta, 6) = 2\cdot10^{-9}$; $L_\infty(\delta, 6) = 5E_\infty\sqrt{E_\infty}/D_\infty = 10$. The influence of the external turbulence on the wake characteristics is here negligible. However, taking it into account permits avoidance of indeterminancy in ratios of the type E^2/D and D/E on the wake outer boundary. The boundary itself was determined from the condition of a smooth conjugate of the wake and background characteristics, namely

$$\left.\frac{\partial E}{\partial y}\right|_{y=\delta}\leqslant 0{,}01\ \frac{E(0,\ x)-E_\infty(x)}{\delta}.$$

The passage over to a system of difference equations was realized by using an implicit Krank–Nicholson finite-difference scheme. The linearized system of algebraic equations was solved successively by the method of scalar factorization. The iterative process was continued until the maximal difference in the turbulent energy between two successive iterations was diminished to 0.1% E_0. The wake width grows with progress downstream. When the number of points in the cross section reaches the value $N = 2N_0 = 100$ the step Δy is doubled and the number of points again becomes equal to N_0, which permits computation of the wake characteristics at any distance from the body.

4. Results

Measurements executed in a number of wake transverse sections for $1 \leq x_1/d \leq 100$ show that two zones can be separated in the flow being investigated. In direct proximity to the body ($x_1/d = 6$) intensive mixing of two streams occurs: the boundary layer on the body and the reactive jet streaming through the slot in the trailing edge. These flows differ substantially in both scale and level of turbulent fluctuation intensity and in the nature of their cross flow distribution. The reactive jet emerging from the slot at a relatively high velocity because of its ejection properties entrains the external flow being formed in the boundary layer of the streamlined body and causes contraction of the wake. Consequently, the wake halfwidth $U(\delta_u) = 0{,}5(U_{max}+U_{min})$ determined by means of the profiled of the axial mean velocity component by starting from the standard relationship $x_1/d = 4$ (Fig. 1.) Substantial inhomogeneity in the pressure distribution is also observed in this domain and the flow parameters depend to a significant extent on the individual geometric singularities of the streamlined body. Starting with $x_1/d \geqslant 6$ the pressure gradient in the wake domain practically vanishes and the change in the characteristics of the turbulent velocity field is subjected to boundary layer regularities and is described by the system (2). The main attention is given to precisely this domain ($x_1/d \geqslant 6$) in this paper also.

From an analysis of the results presented in Figs. 1-3, a deduction can be made about the good agreement between the computational and experimental data concerning the wake halfwidths δ_u and δ_E as well as the damping along the plane of symmetry and the turbulence kinetic energy distribution across the flow and the defect in the mean velocity (δ_E is the wake halfwidth determined by means of the turbulence energy profile from the condition

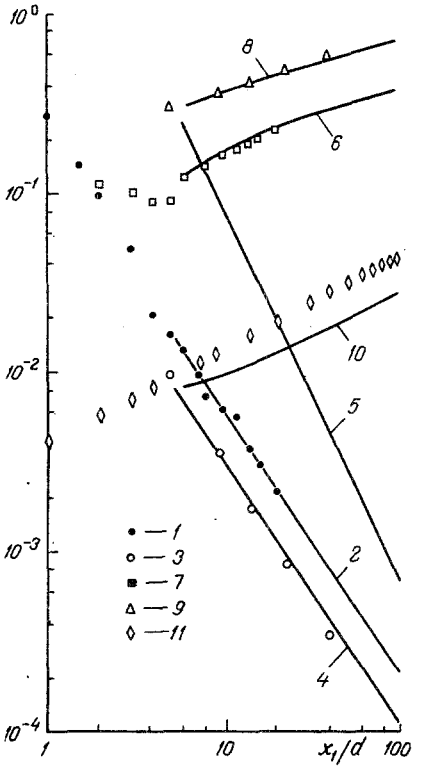

Fig. 1

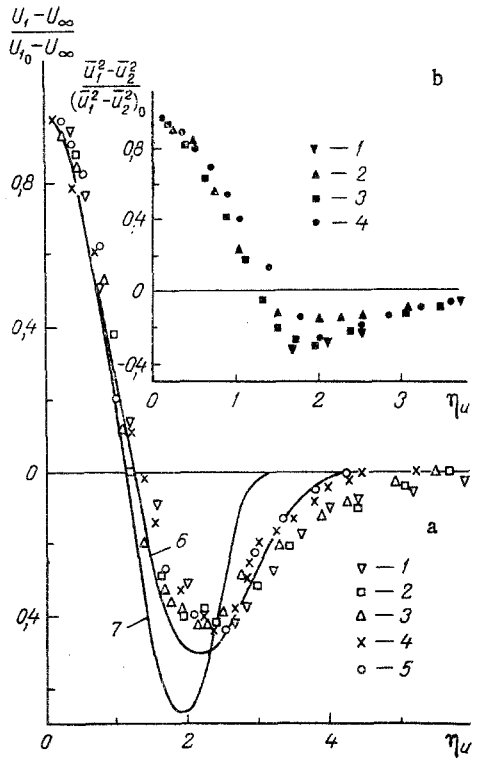

Fig. 2

Fig. 1. Downstream change in the wake parameters: *1, 2* — $\Delta U_0/U_\infty$; *3, 4* — q_0^2/U_∞^2; *5* — $10^3 \cdot \overline{u_1 u_2}/u_\infty^2$; *6, 7* — δ_u/d; *8, 9* — δ_E/d; *10, 11* — $\lambda_0/10\,d$; 1, 3, 7, 9, 11) experiment; 2, 4, 5, 6, 8, 10) computation.

Fig. 2. Distribution of the mean velocity (a) and the normal stress difference (b) across the wake: *a* — *1* — $x_1/d=6$; *2* — 10; *3* — 12; *4* — 14; *5* — 20; *6, 7* — computation (*6* — $x_1/d=10$; *7* — 30); *6* — *1* — $x_1/d=10$; *2* — 14; *3* — 23; *4* — 41.

$E(\delta_E) = 0.25E_0$). As is seen from Fig. 1, the transverse wake dimensions δ_u and δ_E in the self-similar flow domain as well as the velocity defect and turbulence energy vary according to power laws with exponents $n_\delta=0{,}25$; $n_u=n_E=-1{,}5$.

The greatest disagreement between the computed and experimental data is observed for the dissipation function ε, the turbulence scales λ and L, as well as the vortical viscosity $\nu_T = qL$, where

$$L = \frac{5q^3}{\varepsilon} \tag{3}$$

is the Taylor macroscale often names the scale of energy-containing vortices. The quantity $\overline{(\partial u_1/\partial t)^2}$ by which the quantity $\overline{(\partial u_1/\partial x_1)^2}$ was determined on the basis of the Taylor hypothesis was measured directly in the experiment. Then λ and ε were computed:

$$\lambda = [\overline{u_1^2}/\overline{(\partial u_1/\partial x_1)^2}]^{1/2} \text{ and } \varepsilon = 15\nu\,\overline{(\partial u_1/\partial x_1)^2}. \tag{4}$$

Since a locally isotropic approximation (4) was used in determining ε and corrections were introduced to take account of the influence of the limited resolution of the probe filaments, then an attempt was made to estimate the total error in this quantity by using the known integral relation [9].

$$U_\infty \frac{d}{dx_1}\int_0^\infty (\Delta U + q^2)\,dx_2 = -2\int_0^\infty \varepsilon dx_2. \tag{5}$$

Computations using experimental profiles of ΔU, q^2 and ε, as well as dependences of ΔU_0, q_0^2 and δ_E on x_1/d showed that the right side of (5) is approximately 35% less than the left.

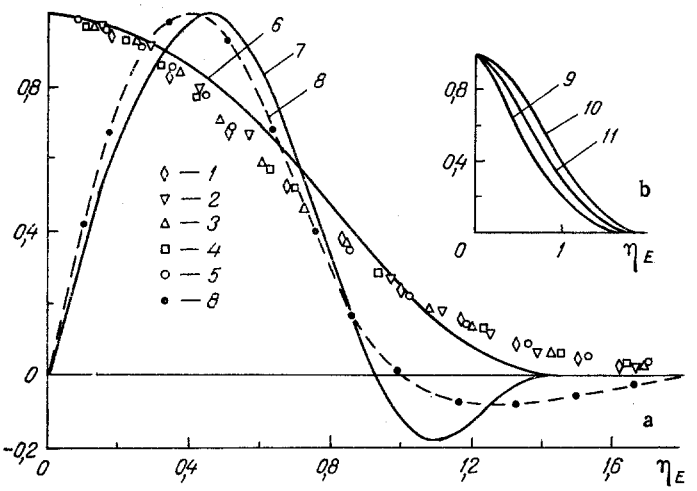

Fig. 3. Transverse distributions of the turbulence energy q^2/q_0^2 (1-6), the tangential $\overline{u_1u_2}/(\overline{u_1u_2})_m$ (7, 8) and normal (9-11) Reynolds stresses; 9—$\overline{u_1^2}/(\overline{u_1^2})_0$; 10—$\overline{u_2^2}/(\overline{u_2^2})_0$; 11—$\overline{u_3^2}/(\overline{u_3^2})_0$; 1—5, 8, 9—11 experiment; 6, 7) self-similar computed profiles ($x_1/d \geqslant 30$); 1—x_1/d=5; 2—10; 3—14; 4—23; 5—41; 8—6.

Without correction of ε in the filament resolution this difference would grow to 50% (in the section $x_1/d = 30$).

Since the experiment does not assure sufficient accuracy of the dissipation velocity measurement ε, then in formulating the initial conditions for the boundary value problem different versions of assigning the profile of ε were provided. It was assumed that the integral in the left side of (5) is determined with acceptable accuracy in the section $x_1/d = 6$, the relationship (5) is satisfied but the form of the transverse distribution of ε can here be different.

It follows from a comparison of the experimental and computed distributions of the dimensionless parameters λ/λ_0, L/L_0 and ν_T/ν_{T0} presented in Fig. 4, that computation yields a different nature in the change of λ across the wake as compared with experiment and, consequently, L and ν_T differing noticeably in the profile shape. The computed profiles here become similar starting with $x_1/d = 30$, while similarity is observed in the experiment at smaller distances from the body. The noticeable differences in the absolute values of the parameters λ_0, L_0, ν_{T0} being compared in the plane of symmetry should also be noted; the dependence of $\lambda_0/10d$ on x_1/d is presented in Fig. 1. The observable differences in the computed and experimental data can be the result of both imperfections in the turbulence model being utilized and illegitimacy in the utilization of the locally isotropic relationships (4). It is interesting to note that if the experimental dissipation profile in the section $x_1/d = 30$ is increased 1.35 times (to satisfy the relationship (5)) then the difference between the computed and experimental values of λ would diminish from 60 to 35%.

Since the defect in the mean velocity decreases rapidly downstream, measurements of the profile of this quantity were performed successfully only for $x_1/d \leq 20$. Good agreement is observed between the experimental and computed data in the wake width δ_u, the downstream damping ΔU_0, as well as in the jet part of the transverse profile (Fig. 2). The computation yields a somewhat reduced value as compared with experiment for the ratio $|\Delta U_{max}/\Delta U_{min}|$. It is here necessary to note that the computed values of the velocity defect presented in the graphs are obtained without taking account of the difference in the normal stresses $R = (R_{11} - R_{22})$ in the momentum equation. The quantity R is determined with large error in the experiment since it is approximately an order of magnitude less than each of the fluctuating velocity components R_{11} and R_{22}. As follows from the measurement results, starting with $x_1/d \geq 14$ the distribution of all three velocity fluctuation components become similar but of noticeably different shape (Fig. 3b). The ratio $(\overline{u_1^2} - \overline{u_2^2})/q_0^2$ along the plane of symmetry here does not diminish in practice, while the change $(\overline{u_1^2} - \overline{u_2^2})$ across the wake in shape recalls the mean velocity profile (Fig. 2b).

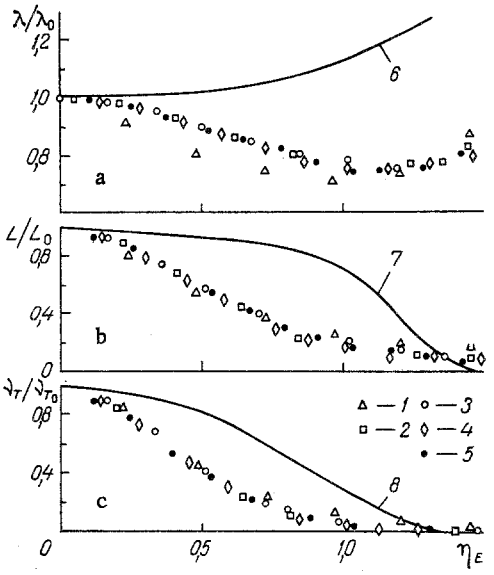

Fig. 4. Transverse microscale (a), macroscale (b), and turbulence viscosity (c) distributions: (1-5) experiment (1) x_1/d = 14; 2) 23; 3) 41; 4) 59; 5) 85; 6-8) self-similar computed profiles ($x_1/d \geq 30$).

It follows from the results of the numerical computations that the exponents in the law of velocity defect generation and the kinematic energy of the turbulent fluctuations are close to each other independently of whether the different in the normal turbulent stresses is taken into account in the momentum equation. For the computations this quantity was assumed proportional to the turbulent energy $(\overline{u_1^2}-\overline{u_2^2})=0{,}1q^2$. The inclusion of this component would result in a certain retardation in the degeneration of the velocity defect ($n_U = -1.4$) and a diminuition in the wake half-width δ_U, however, neither the transverse distribution q^2 nor its damping velocity downstream changed in practice. At the same time taking account of the difference in the normal stresses is of value in principle since it permits finding the connection between the velocity defect damping and the turbulence energy.

The influence of the shape of the transverse dissipation distribution in the initial section (which is equivalent to giving a different scale L) on the evolution of the wake parameters was also investigated during the numerical computations. It turned out that if the magnitude of the integral (5) is conserved unchanged, then the nature of the downstream dumping q^2 also does not change. However, the vortex viscosity profile ν_T changes here, which exerts influence on the degeneration of the velocity defect. As L grows the turbulent diffusion becomes more intensive resulting in an increase in the wake halfwidth. The initial shape of the profile D affects also the distance at which the computed characteristics of D, L and λ become self-similar. However, independently of the initial conditions, the ratio L/δ_E decreases downstream, i.e., the characteristic dimension of the energy-containing vortices grows more slowly than the wake width, which is a result of the rapid decrease in the turbulent Reynolds number R_λ. This is the difference, in principle, between the flow under consideration and the ordinary plane wake (or jet), where the turbulent Reynolds number does not change during degeneration.

An assumption about the constancy of the turbulent viscosity in the wake transverse section is used in theoretical papers [2, 4] to determine the magnitude of the exponents in the damping laws of the wake characteristics. Because of the large errors in the measurements (especially near the extremal points of the velocity defect profile, the $\overline{u_1u_2}$ and U by using the equation $\overline{u_1u_2}=\nu_T\partial U/\partial x_2$. As regards the approximate relationship $\nu_T=c_\mu q^4/\varepsilon$, in both experiment and the computation ν_T has the maximal value in the plane of wake symmetry and decreases in the direction to its periphery (Fig. 4c). Therefore, the assumption about constancy of the vortex viscosity in the flow under consideration is apparently not satisfied.

In conclusion, we note that good agreement between the computed and experimental values of the exponents in the laws of wake parameter evolution downstream with those obtained on the basis of a self-similar analysis [2] is possibly explained by the fact that one of the

exponents (n_δ) in [2] was taken from experiment, which permitted avoidance of additional hypotheses about the constance of ν_T or L across the wake.

NOTATION

U_i, u_i, mean and fluctuating velocity components; U_∞, free stream velocity; $\Delta U = U_1 - U_\infty$, velocity defect; $u_i u_j$, Reynolds stress; $q^2 = \overline{u_i^2}$, twice the kinetic energy of turbulence; $\varepsilon = \nu\overline{(\partial u_i/\partial x_k)^2}$, rate of turbulene energy dissipation; d, maximal vertical body dimension; x_i, Cartesian coordinates; x_1, coordinate along the main flow; x_2, vertical coordinate; λ, Taylor microscale; $\eta_u = x_2/\delta_u$; $\eta_E = x_2/\delta_E$, dimensionless coordinates. Subscript: m, maximal value; 0, value on the axis; ∞, value in the free stream; $\overline{(\ )}$, mean value.

LITERATURE CITED

1. G. Birkhoff and E. Sarantonello, Jets, Wakes, and Caverns [Russian translation], Moscow (1964).
2. V. A. Sabel'nikov, Uch. Zap., TsAGI, 6, No. 4, 71-74 (1975).
3. V. A. Gorodtsov, Izv. Akad. Nauk SSSR, Mekh. Zhidk. Gaza, No. 1, 43-50 (1979).
4. B. A. Kolovandin, Modeling of Heat Transfer in Inhomogeneous Turbulence [in Russian], Minsk (1980).
5. L. N. Ukhanova and M. O. Frankfurt, Inzh.-Fiz. Zh., 47, No. 5, 906-911 (1984).
6. P. Ya. Cherepanov, "Structure of turbulent flows," Coll. Scient. Work, [in Russian], 132-143, Inst. Heat and Mass Transfer, Beloruss. Acad. Sci. (1982).
7. B. A. Kolovandin, N. N. Luchko, Yu. M. Dmitrenko, and V. L. Zhdanov, Turbulent Wake behind an Axisymmetric Body and Its Interaction with External Turbulence, Preprint No. 10 [in Russian], Inst. Heat and Mass Transfer, Beloruss. Acad. Sci., Minsk (1982).
8. B. A. Kolovandin and N. N. Luchko, Heat and Mass Transfer VI, 1, Pt. 2, 126-136 [in Russian], (Materials of the VI All-Union Conference on Heat and Mass Transfer), Inst. Heat and Mass Transfer, Minsk (1980).
9. A. A. Townsend, Structure of a Turbulent Flow with Transverse Shear [Russian translation], Moscow (1959).

MOTION OF VISCOELASTIC LIQUIDS IN A PORous MEDIUM

I. M. Ametov and M. B. Dorfman

UDC 622.276.031:532.13

Nonlinear effects occurring in filtration of viscoelastic liquids are considered. The qualitative differences between one-dimensional and planar cases and between motion in homogeneous and inhomogeneous porous media are demonstrated.

Motion of viscoelastic liquids in a porous medium can be described by a filtration law of the form [1-3]

$$L_1\mathbf{u} = -\frac{k}{\mu}\,\mathrm{grad}\,(L_2 P), \tag{1}$$

where the operators L_1, L_2 have the form

$$L_i = 1 + \sum_{k=1}^{n_i} T_k^i \partial_i^k,$$

where T_k^i are the relaxation time spectra.

These models permit consideration of the unique features of viscoelastic liquid filtration, the major one of which is lengthening of transient processes in the porous medium,

Ukhtin Industrial Institute. Translated from Inzhenerno-Fizicheskii Zhurnal, Vol. 52, No. 5, pp. 751-756, May, 1987. Original article submitted January 31, 1986.

0022-0841/87/5205-0542$12.50